

# Study on the deactivation of supported amorphous Ni-B catalyst in hydrogenation

Zhijie Wu<sup>a</sup>, Minghui Zhang<sup>a,\*</sup>, Wei Li<sup>a</sup>, Shicheng Mu<sup>b</sup>, Keyi Tao<sup>a</sup>

<sup>a</sup> Institute of New Catalytic Materials Science, College of Chemistry, Nankai University, Tianjin 300071, PR China

<sup>b</sup> China National Academy of Nanotechnology & Engineering, Tianjin 300457, PR China

Received 25 December 2006; received in revised form 5 April 2007; accepted 5 April 2007

Available online 8 April 2007

## Abstract

The MgO supported amorphous Ni-B catalyst was synthesized by a modified electroless plating method and its deactivation behavior in the hydrogenation of sulfolene and acetophenone (AP) was studied. The fresh and used catalysts were characterized by inductively coupled plasma atomic emission spectrometry (ICP-AES), X-ray powder diffraction (XRD), transmission electron microscopy (TEM), X-ray photoelectron spectroscopy (XPS), Fourier transform infrared spectra (FT-IR), and hydrogen chemisorption. Carbon disulfide was used to test the sulfur-poison-resistant property of the supported Ni-B/MgO catalyst. No significant sintering of the active component and crystallization of the amorphous structure was found in the hydrogenation. The deactivation of catalyst was ascribed to the sulfur-poisoning by SO<sub>2</sub> in the hydrogenation of sulfolene and the change of porous structure for Ni-B particles in the acetophenone hydrogenation.

© 2007 Elsevier B.V. All rights reserved.

**Keywords:** Amorphous alloy; Ni-B/MgO catalyst; Deactivation; Hydrogenation

## 1. Introduction

Amorphous alloy nanoparticles have received increasing attentions as a novel type of catalytic materials since 1980 [1–3]. Because of the unique isotropic structure and high concentration of coordinatively unsaturated sites, the amorphous alloy catalysts show superior catalytic properties to their crystalline counterparts [1–3]. Especially, the amorphous Ni-B alloy catalyst synthesized by chemical reduction method is superior to normal nickel-based catalysts, such as Raney Ni catalyst in activity, selectivity [4–6] and sulfur-poison-resistant properties [7,8]. Moreover, the thermal stability and cost of the amorphous Ni-B catalyst are improved by depositing Ni-B particles on supports with large surface area [1]. Therefore, various supported amorphous Ni-B catalysts have been prepared and investigated frequently.

Up to the present, the supported amorphous Ni-B catalysts have been mostly prepared by reducing the support impregnated with nickel ions with sodium or potassium borohydride

solution. However, the surface of Ni-B particles synthesized by this method was usually covered with a layer of oxides [9–11], and it was adverse to the promotion of the catalytic properties of catalysts. Chen et al. modified such method by impregnating the mesoporous materials with potassium borohydride, followed by the reaction with nickel chloride solution [12,13]. The modification improved the catalytic properties of supported Ni-B catalysts in the hydrogenation of 2-ethylanthraquinone. In our previous work, we developed a method for synthesizing supported amorphous Ni-B catalysts by a modified silver-catalyzed electroless plating method [13,14]. The resulting catalyst showed superior hydrogenation activity to Raney Ni catalysts and the corresponding supported amorphous Ni-B/MgO catalyst synthesized by the chemical reduction method [13–16]. On the other hand, the practical application of a catalyst not only depended on its catalytic activity, but also on its stability. Therefore, the stability of the supported Ni-B/MgO catalyst in the catalytic reactions was focused in this paper.

For the amorphous Ni-B catalyst, besides the sintering and crystallization of active sites, its stability was also affected by the poison of hydrogenation reactants or products [7,17–19]. The present work emphasized on the investigation of the possible factors responsible for the deactivation of catalysts, such as the

\* Corresponding author. Tel.: +86 22 2350 7730; fax: +86 22 2350 7730.  
E-mail address: [zhangmh@nankai.edu.cn](mailto:zhangmh@nankai.edu.cn) (M. Zhang).

sintering, crystallization, sulfur-poisoning, and oxidation during the catalytic reactions. The results showed that the deactivation of Ni-B/MgO was mainly caused by the sulfur-poisoning and change of the porous structure for Ni-B particles.

## 2. Experimental

### 2.1. Catalyst preparation

The nickel(II) sulfate hexahydrate ( $\text{NiSO}_4 \cdot 6\text{H}_2\text{O}$ ), potassium borohydride ( $\text{KBH}_4$ ), ethylenediamine ( $\text{H}_2\text{NCH}_2\text{CH}_2\text{NH}_2$ ), sodium hydroxide ( $\text{NaOH}$ ), and silver nitrite ( $\text{AgNO}_3$ ) were of reagent grade and used as received. The catalyst was prepared by the silver-catalyzed electroless plating method [13,14] as follows. The MgO support was pretreated by heating to 773 K for 4.0 h, and then Ag/MgO (0.2 Ag wt.%) was prepared according to reference [14]. For the preparation of supported amorphous Ni-B/MgO catalysts, the Ag/MgO was added into 200 mL plating solution with stirring at 323 K until no significant bubbles were observed. The resulting catalyst was washed thoroughly with distilled water until  $\text{pH} = 7$ , then washed with absolute alcohol to remove water and kept in absolute alcohol. The plating solution consisted of nickel(II) sulfate hexahydrate ( $9 \text{ g L}^{-1}$ ), ethylenediamine ( $12 \text{ g L}^{-1}$ ), and potassium borohydride ( $3.75 \text{ g L}^{-1}$ ). The pH value of plating solution was adjusted to 13.5 by sodium hydroxide. The nickel loading was set at 12 wt.%.

### 2.2. Catalyst characterization

The chemical compositions of supported Ni-B catalysts were analyzed by inductively coupled plasma atomic emission spectrometry (ICP-AES) on an IRIS Intrepid spectrometer. The XRD patterns were recorded on a Rigaku D/max 2500 X-ray diffractometer ( $\text{Cu K}\alpha$ ,  $\lambda = 1.54178 \text{ \AA}$ ). Transmission electron microscopy (TEM) images of catalyst were acquired using a JEOL-2010 FEF high resolution transmission electron microscope equipped with an EDX system (EDAX) operating at 200 kV, with a point resolution of 0.23 nm. The selected area electron diffraction (SAED) pattern was taken at 80 kV with a beam size of  $\sim 40 \text{ nm}$  to analyze the crystallinity. The FT-IR spectra were carried out on a NEXUS 870 spectrometer. X-ray photoelectron spectroscopy (XPS) was used to obtain detailed chemical analysis of surface electrical properties from charging studies. The XPS experiments were carried out with a Kratos Axis Ultra DLD spectrometer employing a monochromatic Al  $\text{K}\alpha$  X-ray source, hybrid (magnetic/electrostatic) optics and a multi-channel plate and delay line detector (DLD). To avoid the influence of the surface oxygen, argon etching for 10 min was performed to remove the surface passivation layer.

The active surface area ( $S_{\text{Ni}}$ ) was determined by the hydrogen chemisorption, which was performed by using a dynamic pulse method [8,20–22]. The Ni-B/MgO catalyst was purged by a  $\text{N}_2$  stream (purity of 99.999%) for 1.0 h at 473 K, which was far below its crystallization temperature. Then the sample was cooled to room temperature, and hydrogen pulses were injected at 303 K until the calculated areas of consecutive pulses

became constant. According to the hydrogen chemisorption,  $S_{\text{Ni}}$  and the number of surface Ni atoms were calculated assuming  $\text{H}/\text{Ni}(\text{s}) = 1$  and a surface area of  $6.5 \times 10^{-20} \text{ m}^2$  per Ni atom, based on an average of the areas for the (1 0 0), (1 1 0), and (1 1 1) planes [23].

### 2.3. Catalyst testing

The catalytic hydrogenation was carried out in a 100 mL stainless steel autoclave, equipped with a mass flow controller to record the hydrogen consumption rate during hydrogenations. The effect of stirring was preliminarily investigated. A stirring rate of 800 rpm was employed to eliminate the diffusion limitation. The hydrogen uptake rate, namely the hydrogen consumption per minute, was calculated according to the ideal gas equation.

In the hydrogenation of sulfolene, 1.0 g catalyst (dried at 353 K under 40 mL/min 99.9%  $\text{N}_2$  flow) was transferred into the hydrogenation solution composed of 30.0 mL distilled water and 30.0 g sulfolene. After replacing the air with  $\text{H}_2$  in the reactor, the reaction was performed with 2.0 MPa of hydrogen pressure at 328 K for 100 min.

For the acetophenone (AP) hydrogenation, 1.0 g dry catalyst (treated as above), 6.0 mL AP and 60.0 mL ethanol were mixed. Then the hydrogenation was carried out with 2.0 MPa  $\text{H}_2$  pressure at 343 K for 4.0 h.

The hydrogenation product was filtered to remove the solid catalyst and analyzed by a gas chromatograph equipped with a flame ionization detector (FID).

## 3. Results and discussion

Fig. 1 shows the XRD patterns of the MgO support and supported Ni-B/MgO catalysts. In general, the present study indicates that the amorphous Ni-B alloy shows a broad peak

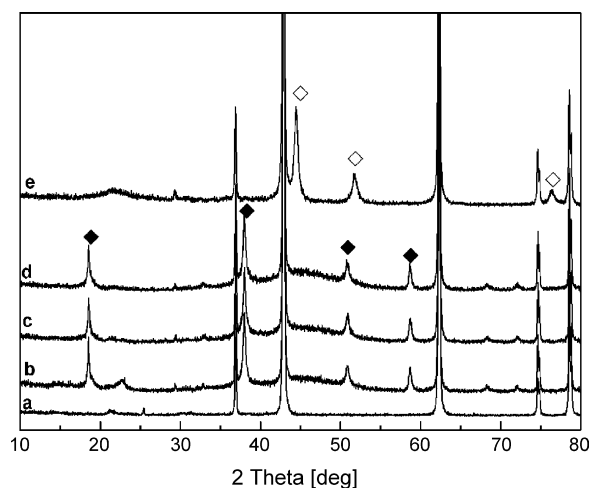


Fig. 1. XRD patterns of different samples: (a) MgO; (b) fresh Ni-B/MgO; (c) Ni-B/MgO used for sulfolene hydrogenation; (d) Ni-B/MgO used for hydrogenation of AP seven times; (e) Ni-B/MgO treated at 773 K under 40 mL/min  $\text{N}_2$  flow for 2.0 h. The peaks of Ni are designated by  $\diamond$ , and the peaks of  $\text{Mg}(\text{OH})_2$  are designated by  $\square$ .

Table 1

The compositions and catalytic activities of Ni-B/MgO catalysts for the hydrogenation of sulfolene

Samples	Nickel loading (wt.%)	$S_{\text{Ni}}$ ( $\text{m}^2/\text{g}$ )	Compositions (atomic ratio)	Conversion of sulfolene (%)
Ni-B/MgO (fresh)	9.8	1.8	$\text{Ni}_{75.2}\text{B}_{24.8}$	98.1
Ni-B/MgO (used) <sup>a</sup>	9.8	0.5	$\text{Ni}_{75.4}\text{B}_{24.6}$	31.2

<sup>a</sup> The Ni-B/MgO (used) was the used catalyst treated as follows: washed with distilled water, ethanol and acetone three times, respectively, then dried at 373 K in a 100 mL/min  $\text{N}_2$  flow for 4.0 h.

around  $2\theta = 45^\circ$  in the XRD patterns, with the complete absence of any sharp crystalline peaks. In comparison to the XRD patterns of the MgO support (Fig. 1a), Ni-B/MgO (Fig. 1b) demonstrates the presence of  $\text{Mg}(\text{OH})_2$ . Furthermore, Ni-B/MgO presents an obvious broad peak around  $2\theta = 45^\circ$  (subtracting the peaks due to MgO), suggesting an amorphous structure of Ni and B. On the other hand, the XRD pattern of the crystalline Ni-B/MgO (Fig. 1e) shows three peaks due to crystalline nickel, indicating the loading of nickel on the support. In short, the XRD patterns reveal that the Ni-B particles over the MgO support are characteristic of the amorphous structure.

### 3.1. Hydrogenation of sulfolene

The hydrogenation of sulfolene to sulfolane is of great industrial importance because sulfolane is widely used as a solvent for both extractions and reactions. Table 1 shows the compositions and catalytic activities of as-prepared Ni-B/MgO catalysts. It is obvious that the load of nickel in the catalyst negligibly changed after the hydrogenation. Fig. 1c shows that the Ni-B particles is still present in the amorphous structure. However, the conversion of sulfolene was 98.1% over a fresh catalyst, while it was 31.2% in the next hydrogenation run. It is due to the sharp decrease in the surface concentration of nickel ( $S_{\text{Ni}}$ ) from  $1.8 \text{ m}^2/\text{g}$  to  $0.5 \text{ m}^2/\text{g}$ . In our view, the decrease in the  $S_{\text{Ni}}$  value should be ascribed to the poison or the change of structure for the Ni-B/MgO catalyst during the hydrogenation.

To study the deactivation in the hydrogenation of sulfolene, various factors, such as the solvent, hydrogenation reactant and product, and hydrogenation temperature and pressure were considered. In our experiments, it has been found that the amorphous Ni-B/MgO catalyst deactivated after the storing in distilled water for several days, while the catalyst in absolute ethanol was stable for several months. Thus, the effect of water on the deactivation of the Ni-B/MgO catalyst was firstly investigated. Wang et al. found that the deactivation of the Ni-B catalyst prepared from the chemical reduction method was due to the surface oxidation of elemental Ni accelerated by forming  $\text{Ni}(\text{OH})_2$  in the presence of water [18]. In this paper, the XPS was used to study the surface properties of fresh catalysts and water-treated Ni-B/MgO catalysts (1.0 g catalyst was stirred with 30 mL distilled water and 2.0 MPa  $\text{H}_2$  at 328 K for 100 min). Fig. 2 shows the XPS spectra of the fresh and treated catalysts. It is notable that a small amount of boron species in the fresh catalyst was present in the oxidized form ( $\text{B}_2\text{O}_3$ ) corresponding to binding energies (BE) of 191.5 eV (Fig. 2a) [24–28]. The NiO are found on the surface of the fresh Ni-B/MgO catalyst; the peaks appear at the

corresponding BE of 855.7 eV, 861.6 eV, 873.5 eV and 879.2 eV (Fig. 2b). After the treatment of fresh Ni-B/MgO with water, the surface amount of  $\text{B}_2\text{O}_3$  and NiO increases remarkably according to the intensity of B 1s and Ni 2p peaks. Moreover, the  $S_{\text{Ni}}$  value of treated catalyst drops slightly from  $1.8 \text{ m}^2/\text{g}$  to  $1.7 \text{ m}^2/\text{g}$ , resulting in decrease in the conversion of sulfolene from 98.1% to 93.2%. As the used catalyst shows only 31.2% conversion of sulfolene (Table 1), it can be concluded that the presence of water leads to the activity decrease of the Ni-B/MgO catalyst, but it is not the main cause of deactivation.

Then the factors related with the Ni-B/MgO catalyst were focused on the hydrogenation reactants and products. Firstly, the fresh Ni-B/MgO catalyst was respectively soaked in sulfolene solution (30 g sulfolene and 30 g distilled water) under  $\text{N}_2$

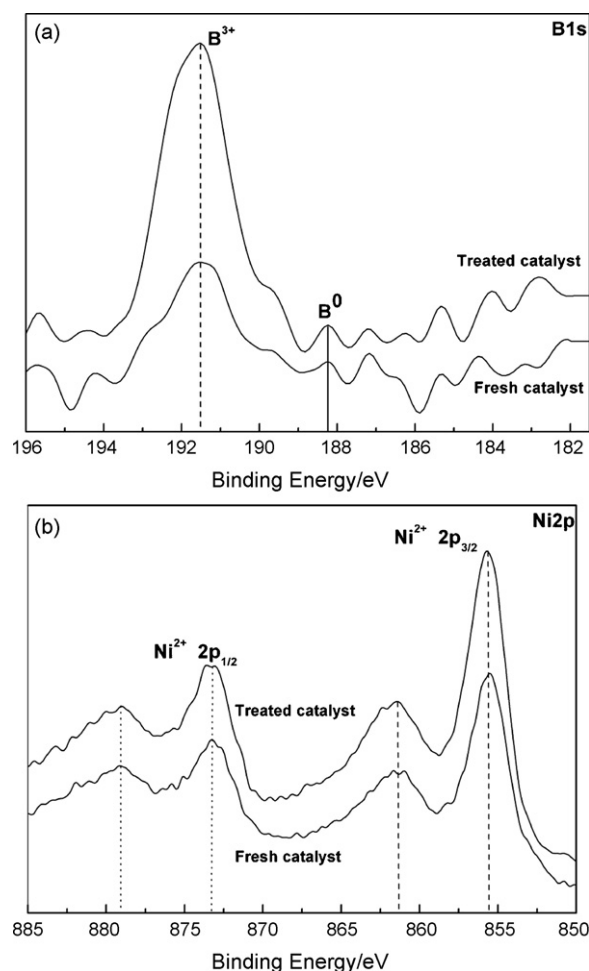


Fig. 2. XPS spectra of (a) B 1s and (b) Ni 2p of Ni-B/MgO.

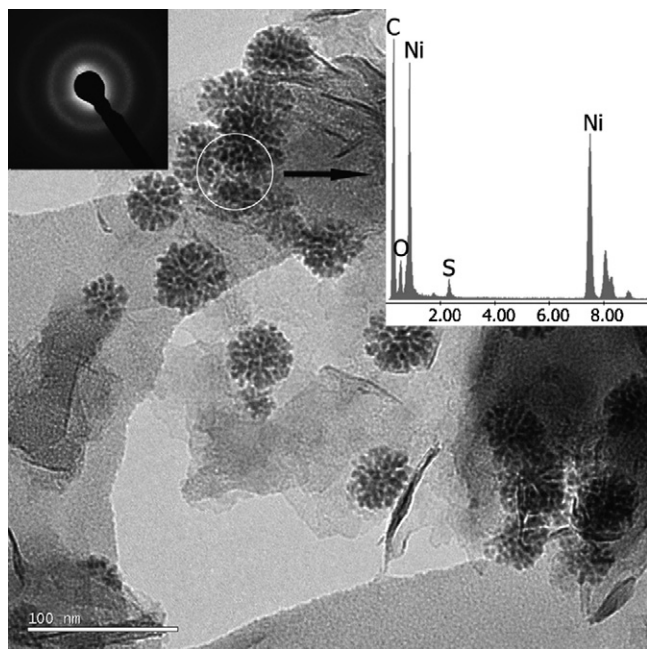


Fig. 3. TEM images of used Ni-B/MgO catalysts. The insets are the SAED pattern and EDS spectra of corresponding circle area.

atmosphere at 328 K and sulfolane solution (30 g sulfolane and 30 g distilled water) in  $H_2$  atmosphere at 328 K for 100 min, and then used in the hydrogenation, respectively. The conversion was 92.7% over the Ni-B/MgO catalyst treated with sulfolene, while it was 92.1% for the catalyst treated with sulfolane. It showed that the activity of Ni-B/MgO was hardly restrained by the hydrogenation reactants and products.

The results above have revealed that the solvent, and hydrogenation reactant and product in hydrogenation showed minor effect on the catalytic activity, and no change of the amorphous structure occurred after hydrogenation. Therefore, the change of Ni-B nanoparticles size and micrograph was studied by the TEM characterization. Fig. 3 shows the TEM images of the used catalyst washed with distilled water, ethanol and acetone thoroughly. The Ni-B nanoparticles  $\sim 40$  nm in sized present in flower-like structure are distributed homogeneously over the support, which is in agreement with the results of fresh Ni-B/MgO catalyst [13,14]. Furthermore, the SAED pattern in the inset of Fig. 3 shows very diffuse rings, which implies that short-range order exists, and that the order is not long enough to give well-defined diffraction pattern. Alternatively, the used Ni-B/MgO catalyst shows an amorphous structure for Ni-B particles like the result of Fig. 1c. The results show that there were no significant sintering of the active component and crystallization of the amorphous structure. However, the EDS result indicates the presence of sulfur adsorbed on the used Ni-B/MgO catalyst.

To study the structure of adsorbed sulfur compound, the IR spectra was used to characterize the fresh catalyst and used catalyst. Fig. 4 shows the IR spectra of sulfolene, sulfolane and catalysts. In our experiments, the catalyst treated with sulfolene and sulfolane was washed with distilled water and ethanol, respectively, before the IR characterization. The IR spectra of the treated catalysts with sulfolene and sulfolane are the same

as that of the fresh Ni-B/MgO (Fig. 4a) catalyst after washing and drying in vacuum. Thus, it could be concluded that the adsorbed sulfur compounds should be the by-product or intermediate of the hydrogenation process. The peaks at  $1130\text{ cm}^{-1}$  and  $1300\text{ cm}^{-1}$  due to vibration of S=O double bond were found in the used catalyst. Besides the above two peaks, the peaks at  $1420\text{ cm}^{-1}$  and  $656\text{ cm}^{-1}$  could all be ascribed to sulfolene or sulfolane. Moreover, a new peak at  $1260\text{ cm}^{-1}$  was found in the spectra. It should be due to the absorption of  $SO_2$  or polymeric sulfones formed during the hydrogenation of sulfolene [29–32].

The production of sulfolane began in England in 1940s: butadiene reacted with  $SO_2$  to synthesize sulfolene, which was then hydrogenated on Ni-based catalyst to produce sulfolane [33]. Generally, the Ni-based catalyst was used only once for the hydrogenation due to the deactivations by  $SO_2$  and polymeric sulfones contained in sulfolene [34–38]. In the present work, the sulfolene was of reagent grade without  $SO_2$  and polymeric sulfones, but the analysis of the hydrogenation product by a gas chromatograph–mass spectrometer (GC–MS) shows the presence of polymeric sulfones. Thus, it can be concluded that the sulfolene would decompose partly into butadiene and sulfur dioxide, or polymerize to heterocyclic sulfones and polymeric sulfones in the hydrogenation of sulfolene, which cause the deactivation of the Ni-B/MgO catalyst. Then the XPS spectra of S-species on the used Ni-B/MgO catalyst was measured as shown in Fig. 5. The surface content of sulfur over the used Ni-B/MgO catalyst is 3.8 wt.%. The binding energies of Ni  $2p_{3/2}$  increased from 855.7 eV and 861.6 eV, for the fresh catalyst, to 858.5 eV and 864.6 eV, for the used catalyst. It suggests that the valence of Ni increased due to the transfer of electrons from Ni atoms to other atoms [39]. Alternatively, the Ni atoms on the surface may form new compounds with other atoms. For the S-species in Fig. 5b, the fitting of S  $2p$  peaks (without fixing either positions or half-widths) gave the following binding energies:  $160.4 \pm 0.1\text{ eV}$ ,  $161.6 \pm 0.2\text{ eV}$ ,  $165.8 \pm 0.2\text{ eV}$  and  $167.3 \pm 0.2\text{ eV}$ . Moreover, the intensity of the peaks at 165.8 eV and 167.3 eV are the strongest compared to other peaks in Fig. 5b. The binding energy of S  $2p$  for  $SO_2$  is generally 166–168 eV [40,41], while that for sulfones C– $SO_2$ –C is

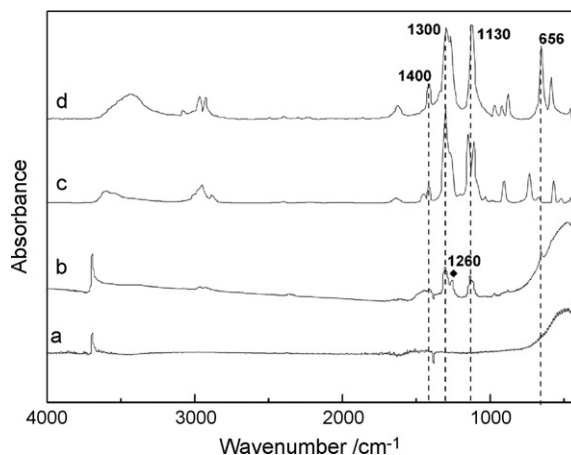


Fig. 4. IR spectra of samples: (a) fresh Ni-B/MgO; (b) used Ni-B/MgO; (c) sulfolane; (d) sulfolene.

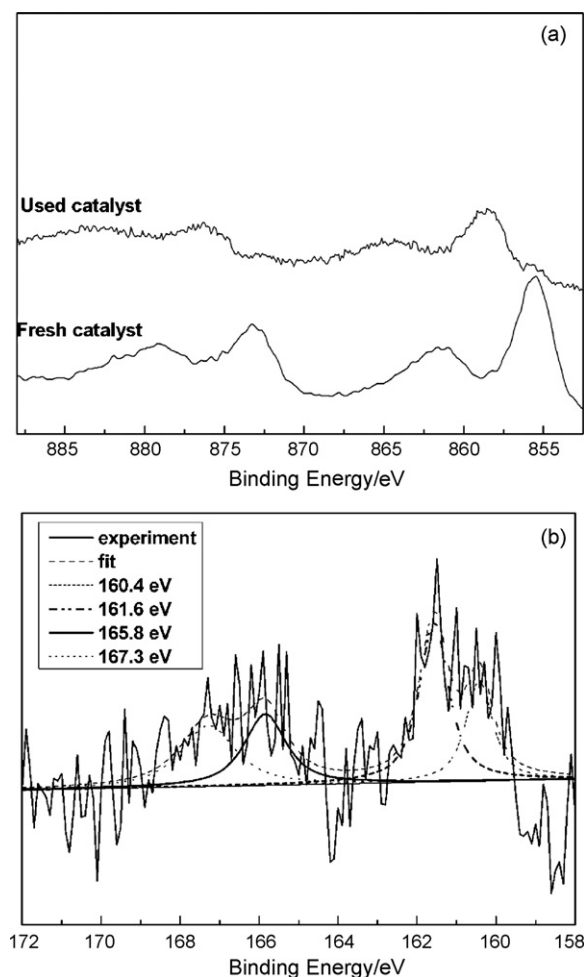


Fig. 5. XPS spectra of the used Ni-B/MgO catalyst: (a) spectra of Ni 2p and (b) spectra of S 2p for used catalyst.

168.3 eV [42,43]. The S-species adsorbed by the catalyst is obviously ascribed to  $\text{SO}_2$  rather than sulfones. As far as the binding energies of 160.4 eV and 161.6 eV are concerned, they should be due to the S-species with the nickel–sulfur bonding [44–46]. The result shows that  $\text{SO}_2$  was adsorbed strongly on the Ni-B/MgO catalyst, which resulted in the formation of nickel–sulfur bonding. The formation of nickel–sulfur bonding led to the increase in the binding energy for Ni-species (Fig. 5a). As it has been pointed out above, the deactivation of the nickel-based catalyst in the hydrogenation of sulfolene was mainly ascribed to the adsorption of  $\text{SO}_2$  and polymeric sulfones [34–38]. Here, the XPS spectra suggest that the deactivation of Ni-B/MgO catalyst is ascribed to the adsorption of  $\text{SO}_2$ , then forming the nickel–sulfur bonding.

As reported in literature, the amorphous Ni-B catalyst synthesized by the chemical reduction method exhibits excellent sulfur-poison-resistance properties. The boron atoms lack electrons by transferring electrons to nickel atoms in Ni-B particles, and they preferentially react with sulfur atoms with lone electron pair [7,17–19]. In this paper, a small amount of  $\text{CS}_2$  was added into the sulfolene solution to evaluate the sulfur-poison-resistance properties of the Ni-B/MgO catalyst synthesized by the electroless plating method to be compared with the conventional

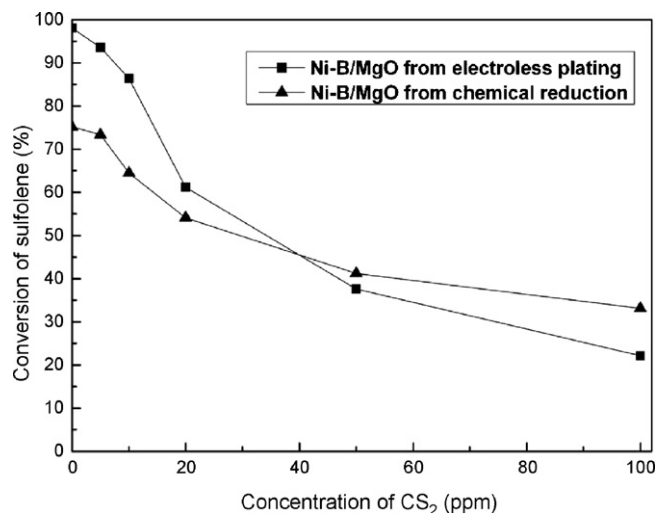


Fig. 6. Relative activity of amorphous Ni-B/MgO catalyst with various  $\text{CS}_2$  concentrations in the feedstock.

chemical reduction method. Fig. 6 shows the effect of  $\text{CS}_2$  on the catalytic activity of Ni-B/MgO during the hydrogenation of sulfolene. In the absence of  $\text{CS}_2$ , the catalytic activity of Ni-B/MgO prepared by the electroless plating method is much higher than that by the chemical reduction method. With the increase in the  $\text{CS}_2$  concentration in hydrogenation solution, the activities of both Ni-B/MgO samples decrease gradually. However, when the amount of  $\text{CS}_2$  increases to  $\sim 40$  ppm, the Ni-B/MgO catalyst synthesized by the chemical reduction method shows superior activity. It means that the  $\text{CS}_2$  results in a much more drop of catalytic activity for the Ni-B/MgO catalyst synthesized by the electroless plating method. It has been reported that the superior sulfur-poison-resistance property of amorphous Ni-B catalysts is possibly attributed to the partial electron transfer from the metalloid boron to the metallic nickel, which makes the Ni active sites electron-enriched while the elemental B becomes electron-deficient [47]. Thus, the boron adsorbs sulfur reversibly in preference to the nickel, protecting the Ni active sites from the sulfur poison [47]. In our work, the composition of Ni-B/MgO

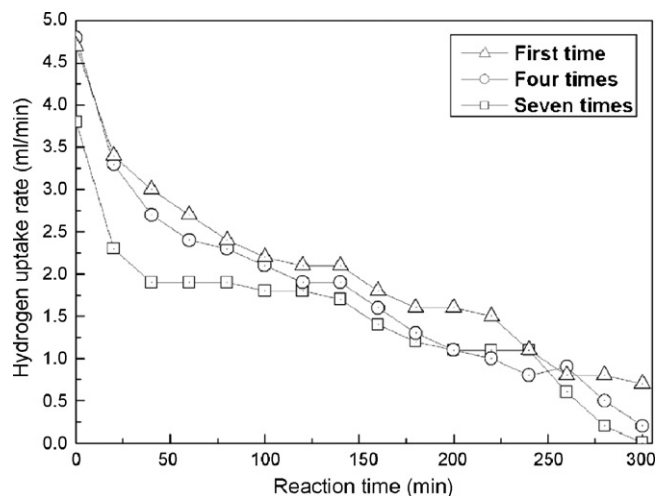


Fig. 7. Hydrogen uptake rates over the Ni-B/MgO catalyst in the hydrogenation of acetophenone.

Table 2  
The catalytic activities of Ni-B catalysts recycled in the hydrogenation of acetophenone (AP)

Sample (time)	Nickel loading (wt.%)	Conversion (%)	Product distribution (% selectivity)	
			1-Phenylethanol (PE)	Ethylbenzene (EB)
Ni-B (first)	9.8	76.1	26.2	45.7
Ni-B (fifth)	9.8	72.1	27.2	45.2
Ni-B (seventh)	9.8	57.2	26.4	45.6

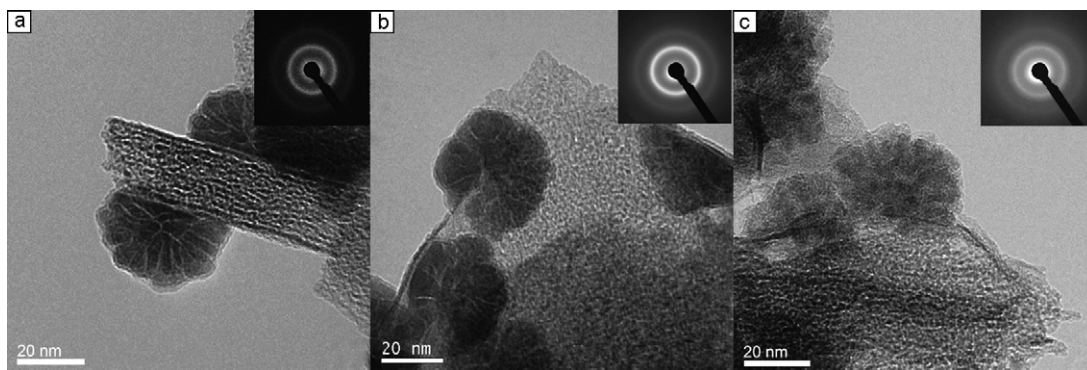


Fig. 8. The HRTEM images of Ni-B/MgO: (a) fresh catalyst; (b) recycled catalyst after the fifth run of hydrogenation; (c) recycled catalyst after the seventh run of hydrogenation. The insets are the SAED patterns corresponding to the fresh and recycled catalysts, respectively.

synthesized by the electroless plating method is  $\text{Ni}_{75.2}\text{B}_{24.8}$ , while that of Ni-B/MgO prepared by the chemical reduction method is  $\text{Ni}_{64.5}\text{B}_{35.5}$ . The result of the  $\text{CS}_2$  deactivation experiment suggests that the lower sulfur-poison-resistance property of Ni-B/MgO prepared by the electroless plating method should be due to the low content of boron in the Ni-B particles.

### 3.2. Acetophenone hydrogenation

The results of sulfolene hydrogenation have shown the sulfur-poisoning on the Ni-B/MgO catalyst. On the other hand, the amorphous Ni-B alloy catalyst was characteristic of the metastable structure [1], which restricts its application in many severe reaction conditions. It has been revealed that water and sulfur compounds were disadvantageous to the Ni-B/MgO catalyst. So the nonaqueous hydrogenation of non-sulfur compounds, such as the hydrogenation of acetophenone (AP), was used to test the stability of the Ni-B/MgO catalyst in catalytic reaction. The hydrogenation of AP is particularly important because of the extensive industrial use of the possible reaction products: 1-phenyl ethanol (PE) [48–50]. In the process of hydrogenation, further hydrogenolysis of PE to styrene usually occurred, leading to the formation of by-product ethylbenzene (EB) [49–51]. Then the yields of PE and EB suggest the ketone hydrogenation activity over Ni-B catalysts in this reaction.

Table 2 summarizes the catalytic activity of hydrogenation of AP and Fig. 7 shows the hydrogen uptake rates over the Ni-B/MgO catalyst. The catalyst can be recycled five times with negligible decrease in the conversion of AP. When the catalyst was recycled seven times, the hydrogenation rate started to fall down as well as the conversion (from 76.1% to 57.2%). The decrease in the hydrogenation rate and conversion was accelerated with increasing times of recycling catalyst, as shown in

Fig. 7. However, the selectivity of ketone hydrogenation is similar, suggesting negligible change of electronic properties of Ni-B particles in catalysts [48–50].

Fig. 8 shows the TEM images of the fresh and recycled Ni-B/MgO catalysts. The particles size of Ni-B particles in fresh Ni-B/MgO is about 35–40 nm, and changes little after the seventh run of hydrogenation. The SAED patterns of fresh and recycled catalysts show that Ni-B particles are amorphous, which can be confirmed by the XRD pattern in Fig. 1d. However, the flower-like porous structure of Ni-B nanoparticles in the fresh catalyst disappears gradually after several runs of hydrogenations as shown in Fig. 8. The change of Ni-B particles is carried out on different areas of the sample to exclude the influence of electron beam [52,53]. With the disappearance of porous structure after the seventh run of hydrogenation, the  $S_{\text{Ni}}$  value decreases sharply to  $0.8 \text{ m}^2/\text{g}$ , compared to  $1.8 \text{ m}^2/\text{g}$  of the fresh one. It means that the deactivation of the Ni-B/MgO catalyst is mainly ascribed to the change of the porous structure of Ni-B particles.

## 4. Conclusions

The deactivation of the supported Ni-B/MgO catalyst synthesized by a silver-catalyzed electroless plating method was studied in the hydrogenation of sulfolene and acetophenone. The TEM images, and IR and XPS spectra revealed that the sulfur-poisoning was the main deactivation factor for the Ni-B/MgO catalyst in the hydrogenation of sulfolene. On the other hand, the performance of the Ni-B/MgO catalyst in the hydrogenation of acetophenone showed that the destruction of the porous structure of Ni-B particles led to the decreased surface concentration of nickel ( $S_{\text{Ni}}$ ), which resulted in the deactivation of catalyst.

## Acknowledgements

The authors acknowledge the financial support of the National Natural Science Foundation of China (Grants 20403009) and the Key Project of Chinese Ministry of Education (No. 105045).

## References

- [1] E.Z. Min, C.Y. Li, *Base of Science and Engineering of Green Petrochemical Technology*, Chinese Petrochem Press, Beijing, 2002.
- [2] Y. Chen, *Catal. Today* 44 (1988) 3.
- [3] J.F. Deng, H.X. Li, W.J. Wang, *Catal. Today* 51 (1999) 113.
- [4] S.H. Xie, H.X. Li, H. Li, J.F. Deng, *Appl. Catal. A: Gen.* 189 (1999) 45.
- [5] H.X. Li, Y.P. Xu, H. Li, J.F. Deng, *Appl. Catal. A: Gen.* 216 (2001) 51.
- [6] H. Li, H.X. Li, J.F. Deng, *Mater. Lett.* 50 (2001) 41.
- [7] W.J. Wang, H.X. Li, J.F. Deng, *Appl. Catal. A: Gen.* 203 (2000) 293.
- [8] H.X. Li, H. Li, W.L. Dai, M.H. Qiao, *Appl. Catal. A: Gen.* 238 (2003) 119.
- [9] K. Molvinger, M. Lopez, J. Court, *J. Mol. Catal. A: Chem.* 150 (1999) 267.
- [10] A. Corrias, G. Ennas, G. Licheri, G. Marongiu, G. Paschina, *Chem. Mater.* 2 (1990) 363.
- [11] G.N. Glavee, K.J. Klabunde, C.M. Sorensen, G.C. Hadjapanayis, *Langmuir* 8 (1992) 771.
- [12] X.Y. Chen, H.R. Hu, B. Liu, M.H. Qiao, K.N. Fan, H.Y. He, *J. Catal.* 220 (2003) 254.
- [13] Z.J. Wu, M.H. Zhang, S.H. Ge, Z.L. Zhang, W. Li, K.Y. Tao, *J. Mater. Chem.* 15 (2005) 4928.
- [14] S.H. Ge, Z.J. Wu, M.H. Zhang, W. Li, K.Y. Tao, *Ind. Eng. Chem. Res.* 45 (2006) 2229.
- [15] L.J. Wang, M.H. Zhang, W. Li, K.Y. Tao, *Chin. J. Catal.* 26 (2005) 91.
- [16] S.H. Ge, Z.J. Wu, M.H. Zhang, W. Li, S.C. Mu, K.Y. Tao, *Chin. J. Catal.* 27 (2006) 690.
- [17] W.J. Wang, H.X. Li, S.H. Xie, Y.J. Li, J.F. Deng, *Appl. Catal. A: Gen.* 184 (1999) 33.
- [18] W.J. Wang, M.H. Qiao, H.X. Li, W.L. Dai, J.F. Deng, *Appl. Catal. A: Gen.* 168 (1998) 151.
- [19] W.J. Wang, H. Li, H.X. Li, Y.J. Li, J.F. Deng, *Appl. Catal. A: Gen.* 203 (2000) 301.
- [20] H.X. Li, W.J. Wang, J.F. Deng, *J. Catal.* 191 (2000) 257.
- [21] W.J. Wang, M.H. Qiao, J. Yang, S.H. Xie, J.F. Deng, *Appl. Catal. A: Gen.* 163 (1997) 101.
- [22] D. Klvana, J. Chaouki, D. Kusohorsky, C. Chavarie, G.M. Pajonk, *Appl. Catal. A: Gen.* 42 (1988) 121.
- [23] C.W. Bartholomew, R.J. Farrauto, *J. Catal.* 45 (1976) 41.
- [24] W.L. Dai, H.X. Li, Y. Cao, M.H. Qiao, K.N. Fan, J.F. Deng, *Langmuir* 18 (2002) 9605–9608.
- [25] J. Legrand, A. Taleb, S. Gota, M.J. Guittet, C. Petit, *Langmuir* 18 (2002) 4131–4137.
- [26] H. Li, H.X. Li, W.L. Dai, J.F. Deng, *Appl. Catal. A: Gen.* 207 (2001) 151–157.
- [27] W.J. Wang, M.H. Qiao, H.X. Li, W.L. Dai, J.F. Deng, *Appl. Catal. A: Gen.* 168 (1998) 151–157.
- [28] Y.M. Chow, W.M. Lau, Z.S. Karim, *Surf. Interface Anal.* 31 (2001) 321–327.
- [29] Z.P. Zhu, Z.Y. Liu, S.J. Liu, H.X. Niu, *Appl. Catal. B* 30 (2001) 267.
- [30] J.E. Bailie, C.H. Rochester, G.J. Hutchings, *J. Mol. Catal. A* 136 (1998) 35.
- [31] S. Kataoka, E. Lee, M.I. Tejedor-Tejedor, M.A. Anderson, *Appl. Catal. B* 61 (2005) 159.
- [32] M.F.R. Fouda, H.I. Saleh, M.M. Abd-Elzاهر, R.S. Amin, *Appl. Catal. A: Gen.* 223 (2002) 11.
- [33] Y.F. Ma, W. Li, M.H. Zhang, Y. Zhou, K.Y. Tao, *Appl. Catal. A: Gen.* 243 (2003) 215.
- [34] M.E. Nash, E.E. Huxley, Patent US 4,286,099 (1981).
- [35] E.E. Huxley, M.E. Nash, Patent US 4,275,218 (1981).
- [36] A.G. Rakhimkulov, U.S. Rysaev, F.T. Rakhmatullina, I.Z. Akhmerov, *Ufimsk. Neft. Inst.* 63 (1990) 1348.
- [37] G.W. Cao, *J. Mol. Catal. (Chin)* 3 (1989) 168.
- [38] Y.R. Gorbenko, S.A. Lange, Z.A. Evdokimova, T.P. Aleksandrova, L.B. Avdeeva, *Neftekhimiya* 12 (1972) 390.
- [39] A. Davidson, J.F. Tempere, M. Che, H. Roulet, G. Dufour, *J. Phys. Chem.* 100 (1996) 4919.
- [40] C.D. Wagner, W.H. Riggs, L.E. Davis, J.F. Moulder, G.E. Muilenberg (Eds.), *A Reference Book of Standard Data for Use in X-ray Photoelectron Spectroscopy*, Perkin-Elmer, Eden-Prairie, 1979.
- [41] C.J. Jackson, D.P. Woodruff, A.S.Y. Chan, R.G. Jones, B.C.C. Cowie, *Surf. Sci.* 577 (2005) 31.
- [42] R. Fiedler, D. Bendler, *Fuel* 71 (1992) 381.
- [43] T. Grzybek, R. Pietrzak, H. Wachowska, *Energy Fuels* 18 (2004) 804.
- [44] R.A. Walton, *Coord. Chem. Rev.* 31 (1980) 183.
- [45] M.C. Bourg, A. Badia, R.B. Lennox, *J. Phys. Chem. B* 104 (2000) 6562.
- [46] Y.W. Yang, L.J. Fan, *Langmuir* 18 (2002) 1157.
- [47] H. Li, H.X. Li, W.L. Dai, W.J. Wang, Z.G. Fang, J.F. Deng, *Appl. Surf. Sci.* 152 (1999) 25.
- [48] M.V. Rajashekharam, I. Bergult, P. Fouilloux, D. Schweich, H. Delmas, R.V. Chaudhari, *Catal. Today* 48 (1999) 83.
- [49] M. Casagrande, L. Storaro, A. Talon, M. Lenarda, R. Frattini, E. Rodríguez-Castellón, P. Maireles-Torres, *Appl. Catal. A: Gen.* 188 (2002) 133.
- [50] J. Masson, P. Cividino, J. Court, *Appl. Catal. A: Gen.* 161 (1997) 191.
- [51] R.V. Malyala, C.V. Rode, M. Arai, S.G. Hegde, R.V. Chaudhari, *Appl. Catal. A* 193 (2000) 71.
- [52] E. Ma, *Pro. Mater. Sci.* 50 (2005) 413.
- [53] L. Xia, M.B. Tang, M.X. Pan, D.Q. Zhao, W.H. Wang, Y.D. Dong, *J. Phys. D: Appl. Phys.* 36 (2003) 2954.